DRAFT VERSION JANUARY 28, 2020
Typeset using LATEX **twocolumn** style in AASTeX62

WASP-4 is Accelerating Towards the Earth

L. G. BOUMA,[1] J. N. WINN,[1] H. ISAACSON,[2] A. W. HOWARD,[3] S. B. HOWELL,[4] AND H. KNUTSON[5]

[1] *Department of Astrophysical Sciences, Princeton University, 4 Ivy Lane, Princeton, NJ 08540, USA*
[2] *Astronomy Department, University of California, Berkeley, CA 94720, USA*
[3] *Cahill Center for Astrophysics, California Institute of Technology, Pasadena, CA 91125, USA*
[4] *NASA Ames Research Center, Moffett Field, CA 94035, USA*
[5] *Division of Geological and Planetary Sciences, California Institute of Technology, Pasadena, CA 91125, USA*

(Received January 28, 2020; Revised —; Accepted —)

Submitted to AAS journals.

ABSTRACT

Space and ground-based transit observations of the hot Jupiter WASP-4b have recently shown that its orbital period is decreasing. Potential causes of the period change include tidal orbital decay, orbital precession, and light-travel time effects. In this work we present new radial velocity measurements of WASP-4, acquired with Keck-HIRES. The new data show that the system is accelerating towards the Earth at $\dot{\gamma} = -0.0422^{+0.0028}_{-0.0027}\,\mathrm{m\,s^{-1}\,yr^{-1}}$. The corresponding period decrease explains WASP-4's changing orbital period as a light-travel time effect. Combining the radial velocities with new speckle imaging limits, we find that system's acceleration is likely caused by a 10-200$\,M_{\rm Jup}$ companion with semi-major axis between 10-100 AU. Based on statistics from Knutson et al. (2014), about 1 in 6 hot Jupiters are expected to show period decreases commensurate with WASP-4 due to acceleration by outer companions. Continued long-term radial velocity monitoring of hot Jupiters is therefore essential to distinguish tidal orbital decay from line-of-sight accelerations.

Keywords: Exoplanet tides (497), Exoplanet dynamics (490), Radial velocity (1332), Transit timing variation method (1710)

1. INTRODUCTION

The issue of whether and how the orbits of hot Jupiters decay due to tidal interaction with their host stars has drawn significant attention over the past 25 years (Rasio et al. 1996; Levrard et al. 2009; Matsumura et al. 2010). Numerous observations have also been performed (CITE). These efforts are now yielding fruit: by combining transit and occultation timing with radial velocity measurements, Yee et al. (2020) have shown that the data for the hot Jupiter WASP-12b are most compatible with orbital decay.

The present study highlights a point that, though obvious, has perhaps not yet received due attention. The point is that observational programs aimed at identifying orbital decay in hot Jupiters will be crippled without long-term radial velocity monitoring programs. The reason is simple: when the timescale of orbital period change exceeds the observing baseline, the first deviation from constant periodicity is always quadratic in the transit number.

Corresponding author: L. G. Bouma
luke@astro.princeton.edu

While orbital decay may be common (CITE). line-of-sight accelerations could be even *more* common (CITE Knutson 14, Bryan 16). Both manifest to first order identically in transit times (up to the sign of the line-of-sight acceleration) – as a non-zero period derivative. Specifically, Knutson et al. (2014) showed that X% of hot Jupiters show some form of radial acceleration in radial velocity time-series with baselines of YY years. Assuming a separation distribution of (WHATEVER), this implies that ZZ% of hot Jupiters will *always* show a changing orbital period, over timescale of say 10 years.

The main focus of this study is the hot Jupiter WASP-4b, which has an orbital period that from transits appears to be decreasing by about 10 milliseconds per year. We discovered the timing variations using data from TESS and a decade of ground-based monitoring (Bouma et al. 2019, hereafter B19). Thereafter, Southworth et al. (2019) reported 22 new transit times for the system, and confirmed that the updated series of transit times was consistent with a quadratic ephemeris. With additional data, they found a lower best-fit decay rate of $\dot{P} = -XX.X \pm X.X$ milliseconds per year. A separate study by Baluev et al. (2019) reported additional archival transit light curves of WASP-4b, most notably from the TRAPPIST archive, and a select few other observers.

To determine the origin of the period change, we acquired four additional radial velocity measurements using Keck-HIRES, extending the RV baseline from 3 to 9 years. Previously, the radial velocities were sparse and showed a weak ($< 2\sigma$) linear trend. Our new measurements reveal a line-of-sight acceleration of $\dot{\gamma} = -0.0422^{+0.0028}_{-0.0027}$ m s^{-1} yr^{-1}. This translates to an expected period decrease simply from the light travel time effect of ZZ milliseconds per year — about commensurate with what is observed. In the following, we avoid the term "Rømer delay" as this phrase typically signifies arrival time delay due to observatory motion. We are discussing an analog of the Doppler effect for a source with constant line-of-sight acceleration.

§ 2 presents the new observations... § 3 describes our analysis... § 4 discusses... § 5 gives conclusions...

2. OBSERVATIONS

2.1. *Transits*

Table N lists the transit times we used in our analysis. We include data from the peer-reviewed literature for which (a) the analysis was based on observations of a single transit, (b) the midpoint was fitted as a free parameter, and (c) the time system specified both the leap second correction (TDB or UTC) and also whether any barycentric or heliocentric corrections had been performed.

The majority of times are identical to those we collected in B19. Twenty-two new times reported by Southworth et al. (2019) are included. These transits were observed from the 3.58m NTT and Danish 1.54m telescopes at La Silla, and the SAAO 1.0m telescope. Additional timimg measurements have also recently been reported by Baluev et al. (2019), based on a homogeneous analysis of archival ground-based observations taken professional and amateur observers. We included twelve of their "high quality" transit times acquired by TRAPPIST (six transits), El Sauce (four transits), and Petrucci et al. (2013). For TRAPPIST and El Sauce, we verified with the original observers that correct barycentric and leap-second corrections had been performed (M. Gillon, P. Evans, priv. comm.). We omitted the fourteen remaining Baluev et al. ETD[1] times due to ambiguity in whether leap-second corrections had or had not been performed.

The four available occultations tabulated by B19 have neglegible statistical value due to their large uncertainties, and we forgo their use in this analysis.

2.2. *Radial velocities*

After identifying the period decrease in B19, we acquired four additional radial velocity measurements with the Keck High Resolution Echelle Spectrometer (HIRES, Vogt et al. 1994). Our observations were acquired under the purview of the California Planet Survey (Howard et al. 2010). The spectra were reduced using **software X**. Previously, the HIRES data-points spanned 2010 to 2013 (Knutson et al. 2014). Our new measurements triple the HIRES observing baseline to nine years.

The complete set of radial velocity observations is given in **Table M**. Along with the 2010-2019 HIRES observations, there are also earlier measurements from CORALIE and HARPS. Following B19, we included the CORALIE measurements from Wilson et al. (2008) and Triaud et al. (2010), using the homogeneous radial velocities calculated by the latter authors. We included the HARPS values reported by Pont et al. (2011) and Husnoo et al. (2012). We omitted the HARPS data points taken over three nights by Triaud et al. (2010) for Rossiter-McLaughlin observations because they have a systematic offset from the remaining datasets.

2.3. *Speckle imaging*

A cursory analysis of the new HIRES observations led to our detection of a linear trend in the residuals after fitting out the orbit of WASP-4b. This prompted us to acquire speckle imaging using Zorro at Gemini-South (see Scott et al. 2018, , and the instrument web-pages[2]). Zorro (and its counterpart, 'Alopeke, on Gemini-North) are dual-channel speckle interferometers that can be used to observe in narrow-band filters centered at 562 nm and 832 nm.

We observed WASP-4 twice, on the night of September 11-12 (8 sets of 1000 frames each) and also on the night of September 28-29 (7 sets of 1000 frames each). The second night had better seeing and produced a slightly better result, which we opt to use for our analysis.

We reduced the speckle images to contrast curves by ...

3. ANALYSIS

3.1. *Transits*

We considered two possible models for the observed transit times. The first model assumes a constant orbital period on a circular orbit:

$$t_{\rm tra}(E) = t_0 + PE, \tag{1}$$

where E is the epoch number and t_0 is a reference epoch. The second model assumes the period changes at a steady rate:

$$t_{\rm tra}(E) = t_0 + PE + \frac{1}{2}\frac{{\rm d}P}{{\rm d}E}E^2. \tag{2}$$

The free parameters are the reference epoch t_0, the period at the reference epoch, and the period derivative, ${\rm d}P/{\rm d}t = (1/P){\rm d}P/{\rm d}E$. We defined the epoch numbers such that $E = 0$ is near the weighted average of the observed times. This helps to reduce the covariance between t_0 and P. A third possible model that we did not consider for reasons that will become apparent is a precessing, eccentric orbit (*e.g.*, Giménez & Bastero 1995; Patra et al. 2017).

We fitted each of the two models by assuming a Gaussian likelihood and sampling over the posterior probability

[1] http://var2.astro.cz/ETD

[2] www.gemini.edu/sciops/instruments/alopeke-zorro/

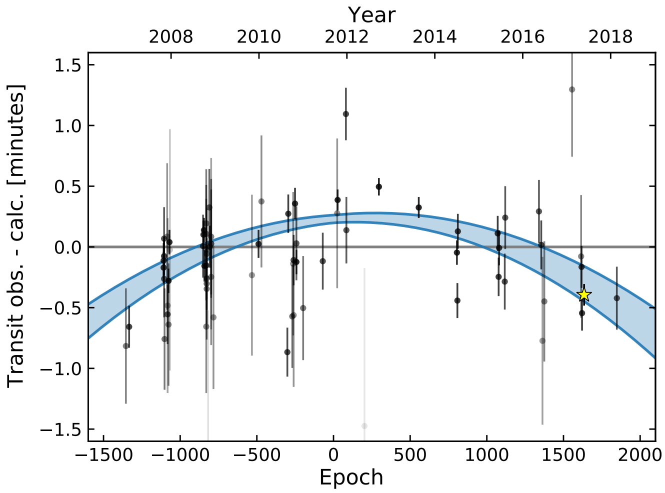

Figure 1. Timing residuals and best-fit models for WASP-4b. The vertical axis shows the observed transit times minus the calculated times assuming a constant orbital period. More opaque points correspond to more precise data. The quadratic ephemeris and its $\pm 1\sigma$ statistical uncertainties are shown in blue. Neither model fully explains the scatter in transit residuals, perhaps due to underestimated uncertainties (see 3.1). The binned TESS point (yellow star) is the weighted average of 18 TESS transits and is binned for display purposes only. Its uncertainty is slightly larger than the marker size. The models were fitted to all of the individual transit times.

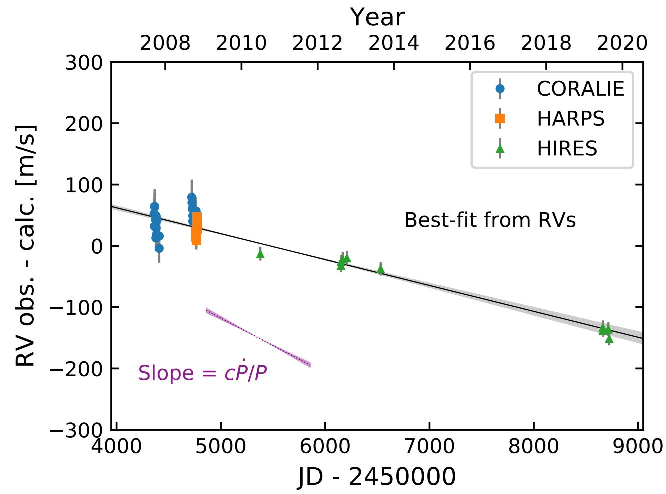

Figure 2. Radial velocity observations of WASP-4. The best-fit Keplerian orbit of WASP-4b has been subtracted. The linear trend inferred from the RV data is shown with a black line, with 1σ errors in gray. The trend that would be needed to produce the period decrease seen in transits ($\dot{P} = -8.64 \pm 0.89$ ms yr^{-1}) is indicated with the purple dotted line. The four new RV measurements presented in this work increased the significance of the radial velocity trend from $\approx 2\sigma$ to 15σ.

distributions. We sampled the posterior using the algorithm proposed by Goodman & Weare (2010) and implemented by Foreman-Mackey et al. (2013) in `emcee`. The prior for the quadratic model allowed the period derivative to have any sign.

Figure 1 shows the observed transit times, minus the best-fit constant period model. The best-fitting constant-period model has $\chi^2 = 276$, 91 degrees of freedom, and $\chi^2_{\rm red} = 3.0$. The best-fitting quadratic model has $\chi^2 = 183$, 90 degrees of freedom, and $\chi^2_{\rm red} = 2.0$. From the reduced χ^2 values, we can surmise that neither model entirely describes the transit data that we have collected—there must be some additional source of signal or potentially noise. In Bouma et al. (2019), we found that the quadratic model for the (less complete) transit data gave $\chi^2_{\rm red} = 1.0$. The only difference between our old and new transit datasets are the addition of transit times from Southworth et al. (2019) and Baluev et al. (2019). The worsened $\chi^2_{\rm red}$ could reflect underestimated statistical uncertainties in these or in fact any of the transit measurements. It could also reflect systematic errors in the time-systems in which the transit measurements were recorded, though we have taken every caution against the latter possibility. The difference in the BIC (Kass & Raftery 1995) between the linear and quadratic and models is ΔBIC = 89.1, strongly favoring the quadratic case.

The best-fit period derivative in the quadratic model is

$$\dot{P} = -(2.74 \pm 0.28) \times 10^{-10} = -8.64 \pm 0.89 \text{ ms yr}^{-1}. \quad (3)$$

This agrees to within 1σ of the value reported by Southworth et al. (2019) ($\dot{P} = -9.2 \pm 1.1$ ms yr^{-1}). It is $\approx 3\sigma$ larger than the rate of period decrease we found earlier (-12.6 ± 1.2 ms yr^{-1}; Bouma et al. 2019), presumably because of missing coverage filled in by Southworth et al.'s and Baluev et al.'s observations. The other best-fit transit timing model parameters are reported in **Table X**.

3.2. *Radial Velocities: WASP-4's acceleration towards the Earth*

We began by fitting a single Keplerian orbit, plus instrument offsets, jitters, and a long-term trend (Fulton et al. 2018, `radvel`). We set Gaussian priors on the period and time of inferior conjunction using the values from Table 4 of B19, and fixed the eccentricity to zero, per the results of Beerer et al. (2011), Knutson et al. (2014) and Bonomo et al. (2017). The free parameters were the velocity semi-amplitude, the instrument zero-points, the instrument jitters (an additive white noise term for each instrument), linear ($\dot{v_{\rm r}}$), and optionally second-order ($\ddot{v_{\rm r}}$) acceleration terms.

We found that the best-fitting model with both linear and quadratic radial velocity terms was marginally preferred (by ΔBIC = 5.8) over the best-fitting model with only a linear term. Regardless, for consistency with Knutson et al. (2014), who fixed the quadratic component of the long-term trend to zero, in Figure 2 we show best-fitting models for the linear-trend case.

WASP-4 was found to be accelerating towards our line-of-sight at high confidence,

$$\dot{v_{\rm r}} = \dot{\gamma} = -0.0422^{+0.0028}_{-0.0027} \text{ m s}^{-1} \text{ day}^{-1}. \quad (4)$$

For comparison, before our recent observing run, $\dot{v_r}$ was thought to be about five times smaller, and was only marginally significant (Knutson et al. 2014; Bouma et al. 2019).

The system's acceleration towards our line-of-sight causes a decrease in the apparent orbital period. The period derivative expected from radial velocities is

$$\dot{P}_{\rm RV} = \frac{\dot{v_r} P}{c} \tag{5}$$

$$\dot{P}_{\rm RV} = -5.94 \pm 0.39 \ {\rm ms\,yr^{-1}}. \tag{6}$$

In other words, the majority of the period decrease observed in transits ($\dot{P} = -8.64 \pm 0.89$ ms yr^{-1}) seems to be explained by the acceleration of the host star.

An important consideration is whether the measured RV trend is at all correlated with stellar activity. We investigate this by analyzing WASP-4's emission in the Ca II H & K lines, as quantified with the chromospheric *S*-index (Wright et al. 2004). We only examined the HIRES velocities for this step, since they are the main source of signal for our analysis. First, we subtracted the orbital solution from the Keck-HIRES velocities. Then, following Bryan et al. (2016, 2019), we calculated the Spearman rank correlation coefficient between the *S*-index and the orbit-subtracted velocities. We found a correlation coefficient of 0.16. Though suggestive, it is not statistically significant (the corresponding *p*-value is 0.65). Furthermore, inspection of the *S*-index timeseries showed no secular or sinusoidal trends, as would be expected if we were observing a long-term magnetic activity cycle. The *S*-index values are included in **Table X**. We conclude that it would be highly unlikely for the linear trend to be caused by stellar activity.

3.3. *Constraints on companion masses and semi-major axes*

Given a linear radial velocity trend, we can place lower-limits on the mass and semi-major axis of additional bodies in the system. As a quick estimate of the minimum mass required to explain the linear trend in WASP-4, we turn to Feng et al. (2015). As they discuss, the scenario that yields the minimum companion mass for a system with a linear trend is a companion with $e \approx 0.5$ and $\omega = 90°$. From their Equation 1,

$$M_{\rm min} \approx 0.0164 M_{\rm Jup} \left(\frac{\tau}{\rm yr}\right)^{4/3} \left|\frac{\dot{\gamma}}{\rm m\,s^{-1}\,yr^{-1}}\right| \left(\frac{M_\star}{M_\odot}\right)^{2/3}, \tag{7}$$

where τ is the observing baseline. For WASP-4, this yields $M_{\rm min} = 4.7 M_{\rm Jup}$. Higher mass companions are allowed, presuming that they orbit further from the star; at fixed $\dot{\gamma}$, $M_{\rm comp} \propto a^2$ (Torres 1999; Liu et al. 2002).

High-resolution images can further limit the available parameter space by setting an upper limit on the semimajor axis, and a maximum brightness (and thereby mass) of any putative companions. The procedure we use to combine constraints from both radial velocities and high resolution imaging has been developed by Wright et al. (2007), Crepp et al. (2012), Montet et al. (2014), Knutson et al. (2014), Bryan et al. (2016, 2019), and others.

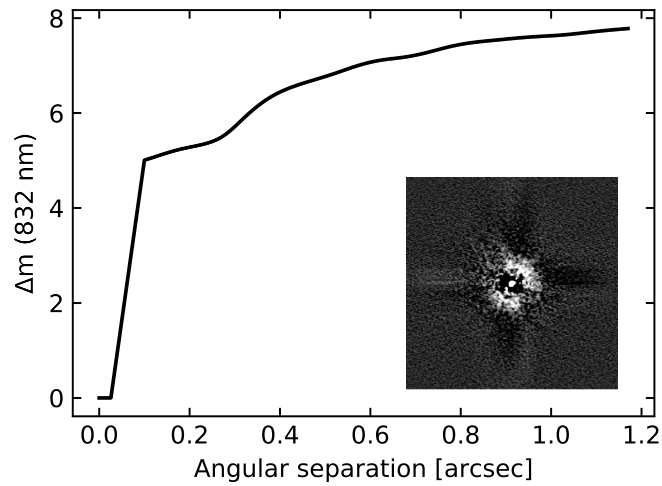

Figure 3. Zorro contrast curve derived from point-source injection-recovery experiments. Sources below the curve would have been detected. The inset shows the speckle image reconstructed from 1000 40 millisecond frames in an 832 nm bandpass, and acquired on September 28, 2019. The image scale is $2.46'' \times 2.46''$.

Speckle imaging constraints—First, we would like to convert the contrast ratios obtained through the Zorro imaging (Figure 3) to limits on the masses of putative companions and their separations from the host star.

To do this, we followed Montet et al. (2014), and opted to employ the Baraffe et al. (2003) models for substellar mass objects and the MIST isochrones for stellar mass objects (Paxton et al. 2011, 2013, 2015; Dotter 2016; Choi et al. 2016). We assumed that the system age was 5 Gyr, so that companions would have fully contracted.

Due to the custom filters of the Zorro imager, and corresponding lack of synthetic photometry, we further assumed that all sources had blackbody spectra. While this is clearly false, we do not readily have access to the planetary and stellar atmosphere models needed for the consistent calculation with the `COND03` and `MESA` models. We therefore adopted the effective temperatures and bolometric luminosities from the Baraffe et al. (2003) and MIST isochrones. Using these theoretical quantities and the empircal Zorro bandpass functions, we calculated absolute magnitudes in the 562 and 832 nm Zorro bandpasses for stellar and planetary mass companions. Applying the same calculation to WASP-4 itself using the effective temperature and bolometric luminosity from B19, we derived the transformation from contrast ratio to companion mass. The resulting limits are shown as the cross-hatched region in Figure 4.

Radial velocity constraints—To derive constraints on possible companion masses and separations from the radial velocities, we mostly followed the procedure of Bryan et al. (2019).

We began by defining a 128×128 grid in true planetary mass and semimajor axis, with even logarithmic spacing from 1 to $900 M_{\rm Jup}$ and 3 to 500 AU. We then considered

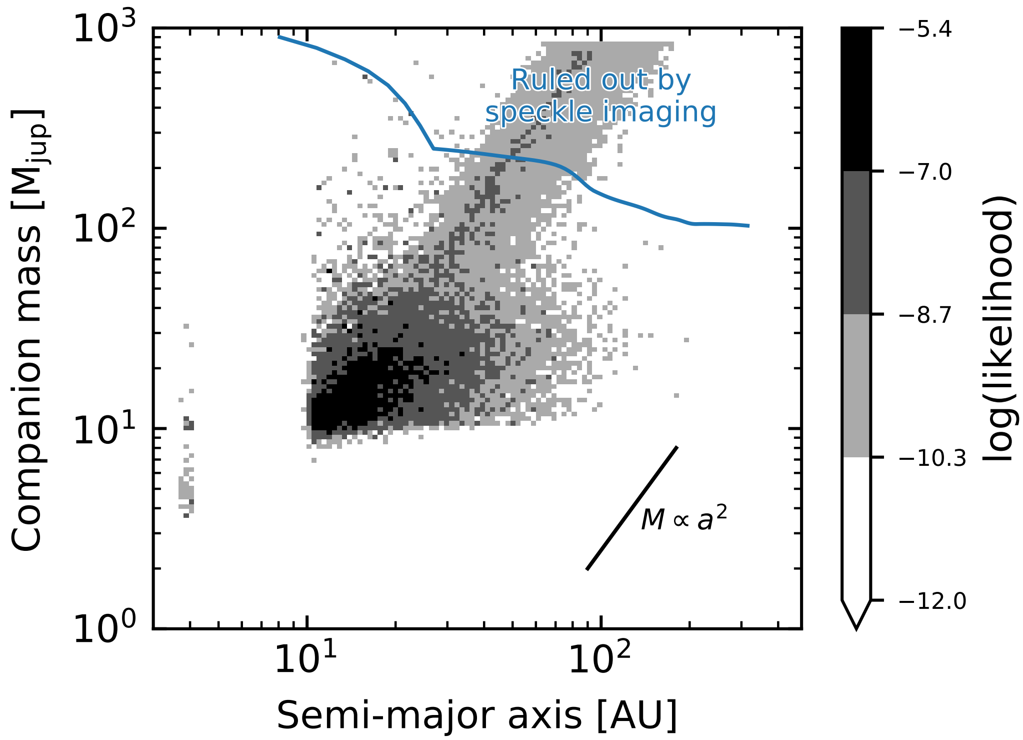

Figure 4. Masses and semi-major axes of companions that meet requirements of both the radial velocity and the speckle imaging. The likelihood inferred from radial velocities is shown in grayscale, and the region excluded from the imaging is shown with a cross-hatch pattern.

the possibility that an additional companion in any particular cell could explain the observed linear trend. In each cell, we simulated 512 hypothetical companions.

We assigned each companion a mass and semimajor axis from log-uniform distributions within the grid cell. We drew the inclination from a uniform distribution in $\cos i$. For companion masses less than $10 M_{\rm Jup}$, we drew the eccentricity from Kipping (2013)'s long-period exoplanet Beta distribution (a = 1.12, b = 3.09). If the companion mass exceeded $10 M_{\rm Jup}$, we drew the eccentricity distribution from the power-law $p_e \propto e^\eta$ reported by Moe & Stefano (2017) in their Equation 17. We emphasize that the long-period exoplanet and long-period binary distributions are quite different: the exoplanet distribution is "bottom-heavy", with eccentricities preferentially close to zero. The binary star distribution is "top-heavy", with more eccentricities close to one. We chose a mass cutoff of $10 M_{\rm Jup}$ based on the bound observed by Schlaufman (2018) between giant planets, presumably formed through core accretion, and brown dwarfs, presumably formed via gravitational instability.

For each simulated companion, we then drew a sample from the converged chains of our initial model of WASP-4b, plus its linear trend. We subtracted the planet's orbital solution, leaving the linear trend. Given (a_c, M_c, e_c for each simulated outer companion, and the fixed instrument offsets and jitters from the MCMC chains, we then performed a maximum likelihood fit for the time and argument of periastron of the outer simulated companion. We converted the resulting $128 \times 128 \times 512$ cube of best-fit log-likelihood values to probabilities, and averaged over the samples in each grid cell to derive a probability distribution in mass and semi-major axis.

The result is shown as grayscale background in Figure 4.

4. DISCUSSION

4.1. *Implications for WASP-4*

Previous possibilities suggested to explain the period decrease of WASP-4b included tidal orbital decay, orbital precession, and light-travel time effects (Bouma et al. 2019). Our new radial velocity measurements have now shown the least exotic option—light-travel time effects—is also the most likely explanation. Transits show the obital period to decrease by $YY.Y \pm Z.Z$ ms yr^{-1}; the line-of-sight acceleration observed in radial velocities implies an expected period decrease of $YY.Y \pm Z.Z$ ms yr^{-1}. Though the quantitative agreement is not perfect, Occam's razor would suggest that the line of sight acceleration is probably a sufficient explanation for the apparent decrease of WASP-4b's orbital period.

The corresponding requirements for the companion causing the acceleration are that it is likely either a brown-dwarf or low mass star, and that it is between 10-100 AU from the host star (Figure 4). Given such a mass, this companion could at one time have influenced the orbital evolution of the inner giant. Further radial velocity monitoring should eventually reveal the orbital parameters and minimum mass of the companion.

4.2. *How many other hot Jupiters are accelerating towards the Earth?*

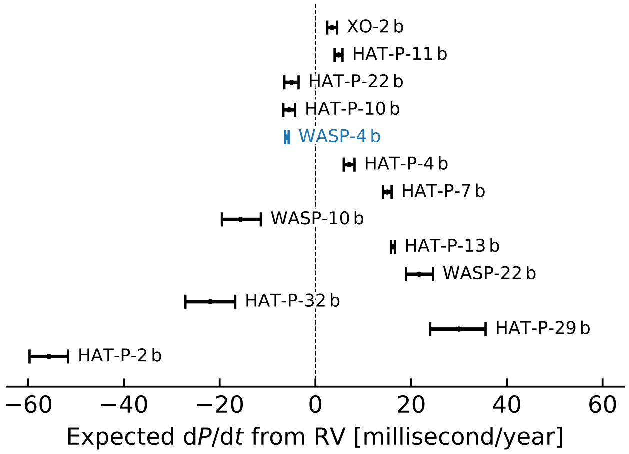

Figure 5. Predicted hot Jupiter period changes from linear radial velocity trends. Including WASP-4b, 16 of 51 hot Jupiters from Knutson et al. (2014) have shown long-term radial velocity trends. The HAT-P-11 signal is plotted, though its radial velocity signal may be caused by stellar activity. Three hot Jupiters are not plotted because their radial velocity curves better described as quadratic trends in time: HAT-P-17, WASP-8, and WASP-34. Objects are ordered in the y dimension by the absolute value of $\mathrm{d}P/\mathrm{d}t$.

We identified WASP-4b's decreasing orbital period as part of a search for tidal orbital decay. However, over half of hot Jupiters have companions outside of 1 AU with super-Jovian masses (Knutson et al. 2014). Line-of-sight accelerations are therefore relatively common in hot Jupiter systems.

To evaluate the importance of these effects in future transit timing searches, we collected the linear trends reported by Knutson et al. (2014), and computed the expected orbital period derivatives $\dot{P}_{\rm RV} = \dot{v}_{\rm r} P/c$ for all the systems. The results are given in **Table X**, and visualized for hot Jupiters with significant linear trends in Figure 5.

Including WASP-4b, 16 of 51 hot Jupiters from Knutson et al. (2014) show a non-zero radial velocity trend. About half are positive, and half are negative, and therefore ≈1 in 6 hot Jupiters are expected to show period decreases commensurate with WASP-4 due to acceleration by outer companions.

5. CONCLUSIONS

We found that WASP-4 is accelerating towards the Earth, at X.XX m/s/yr. This seems like the most plausible explanation for the orbital period decrease observed in transits — not tidal orbital decay, or apsidal precession. The most likely parameters for the companion are XXX. Over half of hot Jupiters have super-Jovian outer companions, so the light-travel time effect will become an increasingly large nuisance in the hunt for orbital decay as the observing baselines for hot Jupiters increase. The requirement to avoid missing out is to have long-term radial velocity monitoring with the same spectrograph (or else to calibrate instrumental offsets by observing the same stars simultaneously).

Software: `astrobase` (Bhatti et al. 2018), `astroplan` (Morris et al. 2018), `astropy` (Collaboration et al. 2018), `astroquery` (Ginsburg et al. 2018), `corner` (Foreman-Mackey 2016), `emcee` (Foreman-Mackey et al. 2013), `IPython` (Pérez & Granger 2007), `matplotlib` (Hunter 2007), `MESA` (Paxton et al. 2011, 2013, 2015) `numpy` (Walt et al. 2011), `pandas` (McKinney 2010), `radvel` (Fulton et al. 2018), `scipy` (Jones et al. 2001).

Table 1. Best-fit transit timing model parameters.

Parameter	Median Value (Unc.)[a]
Constant period	
t_0 [BJD$_{\rm TBD}$]	2455804.515752(+19)(-19)
P [days]	1.338231466(+23)(-22)
Constant period derivative	
t_0 [BJD$_{\rm TBD}$]	2455804.515918(+24)(-24)
P [days]	1.338231679(+31)(-31)
dP/dt	$-4.00(+37)(-38) \times 10^{-10}$

[a] **FIXME table needs numbers** The numbers in parenthesis give the 68% confidence interval for the final two digits, where appropriate.

REFERENCES

Baluev, R. V., Sokov, E. N., Jones, H. R. A., et al. 2019, arXiv:1908.04505 [astro-ph], arXiv: 1908.04505

Baraffe, I., Chabrier, G., Barman, T. S., Allard, F., & Hauschildt, P. H. 2003, A&A, 402, 701

Beerer, I. M., Knutson, H. A., Burrows, A., et al. 2011, ApJ, 727, 23

Bhatti, W., Bouma, L. G., & Wallace, J. 2018, `astrobase`

Bonomo, A. S., Desidera, S., Benatti, S., et al. 2017, A&A, 602, A107

Bouma, L. G., Winn, J. N., Baxter, C., et al. 2019, AJ, 157, 217

Bryan, M. L., Knutson, H. A., Lee, E. J., et al. 2019, AJ, 157, 52

Bryan, M. L., Knutson, H. A., Howard, A. W., et al. 2016, ApJ, 821, 89

Choi, J., Dotter, A., Conroy, C., et al. 2016, ApJ, 823, 102, arXiv: 1604.08592

Collaboration, T. A., Price-Whelan, A. M., Sipőcz, B. M., et al. 2018, arXiv:1801.02634 [astro-ph], arXiv: 1801.02634

Crepp, J. R., Johnson, J. A., Howard, A. W., et al. 2012, ApJ, 761, 39

Dotter, A. 2016, ApJS, 222, 8

Feng, Y. K., Wright, J. T., Nelson, B., et al. 2015, The Astrophysical Journal, 800, 22

Foreman-Mackey, D. 2016, The Journal of Open Source Software, 24

Foreman-Mackey, D., Hogg, D. W., Lang, D., & Goodman, J. 2013, PASP, 125, 306

Fulton, B. J., Petigura, E. A., Blunt, S., & Sinukoff, E. 2018, arXiv:1801.01947 [astro-ph], arXiv: 1801.01947

Giménez, A., & Bastero, M. 1995, Ap&SS, 226, 99

Ginsburg, A., Sipocz, B., Madhura Parikh, et al. 2018, Astropy/Astroquery: V0.3.7 Release

Goodman, J., & Weare, J. 2010, Communications in Applied Mathematics and Computational Science, 5, 65

Howard, A. W., Johnson, J. A., Marcy, G. W., et al. 2010, ApJ, 721, 1467

Hunter, J. D. 2007, Computing in Science & Engineering, 9, 90

Husnoo, N., Pont, F., Mazeh, T., et al. 2012, MNRAS, 422, 3151

Jones, E., Oliphant, T., Peterson, P., et al. 2001, Open source scientific tools for Python

Kass, R. E., & Raftery, A. E. 1995, Journal of the American Statistical Association, 90, 773

Kipping, D. M. 2013, MNRAS:l, 434, L51

Knutson, H. A., Fulton, B. J., Montet, B. T., et al. 2014, ApJ, 785, 126

Levrard, B., Winisdoerffer, C., & Chabrier, G. 2009, ApJ, 692, L9

Liu, M. C., Fischer, D. A., Graham, J. R., et al. 2002, The Astrophysical Journal, 571, 519

Matsumura, S., Peale, S. J., & Rasio, F. A. 2010, ApJ, 725, 1995

McKinney, W. 2010, in Proceedings of the 9th Python in Science Conference, ed. S. van der Walt & J. Millman, 51

Moe, M., & Stefano, R. D. 2017, The Astrophysical Journal Supplement Series, 230, 15

Montet, B. T., Crepp, J. R., Johnson, J. A., Howard, A. W., & Marcy, G. W. 2014, ApJ, 781, 28

Morris, B. M., Tollerud, E., Sipőcz, B., et al. 2018, AJ, 155, 128

Patra, K. C., Winn, J. N., Holman, M. J., et al. 2017, AJ, 154, 4

Paxton, B., Bildsten, L., Dotter, A., et al. 2011, ApJS, 192, 3

Paxton, B., Cantiello, M., Arras, P., et al. 2013, ApJS, 208, 4

Paxton, B., Marchant, P., Schwab, J., et al. 2015, ApJS, 220, 15

Pérez, F., & Granger, B. E. 2007, Computing in Science and Engineering, 9, 21

Petrucci, R., Jofré, E., Schwartz, M., et al. 2013, ApJL, 779, L23

Pont, F., Husnoo, N., Mazeh, T., & Fabrycky, D. 2011, MNRAS, 414, 1278

Rasio, F. A., Tout, C. A., Lubow, S. H., & Livio, M. 1996, The Astrophysical Journal, 470, 1187

Schlaufman, K. C. 2018, arXiv:1801.06185 [astro-ph], arXiv: 1801.06185

Scott, N. J., Howell, S. B., Horch, E. P., & Everett, M. E. 2018, PASP, 130, 054502

Southworth, J., Dominik, M., Jorgensen, U. G., et al. 2019, arXiv:1907.08269 [astro-ph], arXiv: 1907.08269

Torres, G. 1999, Publications of the Astronomical Society of the Pacific, 111, 169

Triaud, A. H. M. J., Collier Cameron, A., Queloz, D., et al. 2010, A&A, 524, A25

Vogt, S. S., Allen, S. L., Bigelow, B. C., et al. 1994, SPIE Conference Series, Vol. 2198, SPIE Conference Series, ed. D. L. Crawford & E. R. Craine, 362

Walt, S. v. d., Colbert, S. C., & Varoquaux, G. 2011, Computing in Science & Engineering, 13, 22

Wilson, D. M., Gillon, M., Hellier, C., et al. 2008, ApJL, 675, L113

Wright, J. T., Marcy, G. W., Butler, R. P., & Vogt, S. S. 2004, ApJS, 152, 261

Wright, J. T., Marcy, G. W., Fischer, D. A., et al. 2007, ApJ, 657, 533

Yee, S. W., Winn, J. N., Knutson, H. A., et al. 2020, The Astrophysical Journal Letters, 888, L5